Chapter 5

Production and Decay of Z Bosons

Operating the LEP storage ring in the vicinity of the Z mass with high luminosity permits a detailed study of the lineshape of the Z resonance. We have performed measurements of the following reactions:

1. $e^+e^- \to$ hadrons,
2. $e^+e^- \to \mu^+\mu^-(\gamma)$,
3. $e^+e^- \to \tau^+\tau^-(\gamma)$,
4. $e^+e^- \to e^+e^-(\gamma)$,
5. $e^+e^- \to$ hadrons $+ \gamma$,
6. $e^+e^- \to \nu\bar{\nu}\gamma$.

The measured cross sections are used to extract the properties of the Z boson: the mass, the total width and its hadronic and leptonic decay widths. Further information on electroweak parameters such as the vector and axial vector coupling constants g_V and g_A is contained in the measurements of the forward-backward asymmetries of the leptonic decay channels of the Z. The difference between the total width and the sum of the observable partial widths, which in the Standard Model is attributed to the Z decays into neutrinos, leads to a determination of the number of light neutrino families. The process $Z \to \nu\bar{\nu}\gamma$ is also directly observed and its rate measured. Interpreted in terms of the predicted width per neutrino family this gives a second, independent measurement of the same quantity [23]. Hard isolated photons in hadronic events can be used to give a measurement of electroweak couplings to up-type and down-type quarks separately.

For all cross section and asymmetry measurements detailed studies of the systematic uncertainties have been carried out. The understanding of the systematic errors is very important to fully exploit the statistical precision achievable by the large number of events collected. The events for all reactions studied, except $\nu\nu\gamma$, are triggered by at least two independent level-1 triggers. For instance, hadronic Z decays are triggered by the energy, scintillation counter and charged particle triggers. Therefore, we can determine individual trigger efficiencies from selected events. From these analyses we find for all reactions a combined trigger efficiency larger than 99.9%. The systematic errors due to trigger inefficiencies are therefore negligible.

In this chapter we briefly describe the analysis methods used for reactions 1–6. More details

can be found in reference 24. We present the cross sections and forward-backward asymmetries obtained in 1991 and the results of the re-analysis of the previously published [24] data taken in 1990 using similar selection criteria and cuts as for the analysis of the data taken in 1991.

5.1 The reaction $e^+e^- \rightarrow$ hadrons

The selection of hadronic Z decays is based on the energy deposition in the electromagnetic and hadron calorimeters. For the measurement of the total cross section we use the following criteria:

1. $0.5 < E_{\rm vis}/\sqrt{s} < 1.5$, where $E_{\rm vis}$ is the total calorimetric energy observed in the detector.
2. $|E_\parallel|/E_{\rm vis} < 0.6$, where $E_\parallel$ is the energy imbalance along the beam direction.
3. $E_\perp/E_{\rm vis} < 0.5$, where $E_\perp$ is the transverse energy imbalance.
4. The number of energy clusters, $N_{\rm cluster}$, reconstructed in the calorimeters is required to satisfy:
   a. $N_{\rm cluster} \geq 13$ for $|\cos\theta_t| < 0.74$ (barrel) or
   b. $N_{\rm cluster} \geq 17$ for $|\cos\theta_t| > 0.74$ (endcap)
   ($N_{\rm cluster} \geq 9$ for 1990 data)

   where θ_t is the polar angle of the event thrust axis (see equation 10.1) with respect to the beam line.

Figure 5.1 shows the distribution of $E_{\rm vis}/\sqrt{s}$ after cuts 2–4 have been applied. The agreement between data and Monte Carlo generated events is very good in the signal region. The background in the sample of hadronic events selected by the above cuts is very small. From the analysis of $e^+e^- \rightarrow \tau^+\tau^-(\gamma)$ and $e^+e^- \rightarrow e^+e^-(\gamma)$ Monte Carlo simulations we derive a background contribution of $(0.10 \pm 0.02)\%$ and 0.02%, respectively. The non-resonant background from beam-gas interactions and two-photon events has been estimated by studying the observed event rate in the region $0.2 < E_{\rm vis}/\sqrt{s} < 0.5$ at different center of mass energies. This leads to an additional contamination of (30 ± 10) pb which amounts to 0.1% of the cross section measured at the Z-peak.

Since the hadron calorimeter covers 99.5% of the full solid angle the acceptance for $e^+e^- \rightarrow$ hadrons events is very high, $(99.15 \pm 0.03)\%$ including all detector inefficiencies. This number has been determined with the JETSET 7.3 [25] Monte Carlo program. An alternative fragmentation model (HERWIG 5.3 [26]) gives the same result within errors. We estimate a 0.1% systematic uncertainty of the acceptance on the Z peak. The extrapolation of the acceptance to the off-peak energies adds a further 0.1% to the systematic error.

To study the dependence of the measured cross section on the selection criteria we have varied our cuts within reasonable limits. Due to the very good agreement of data and Monte Carlo distributions the uncertainty is estimated to be less than 0.15%. We have calculated the

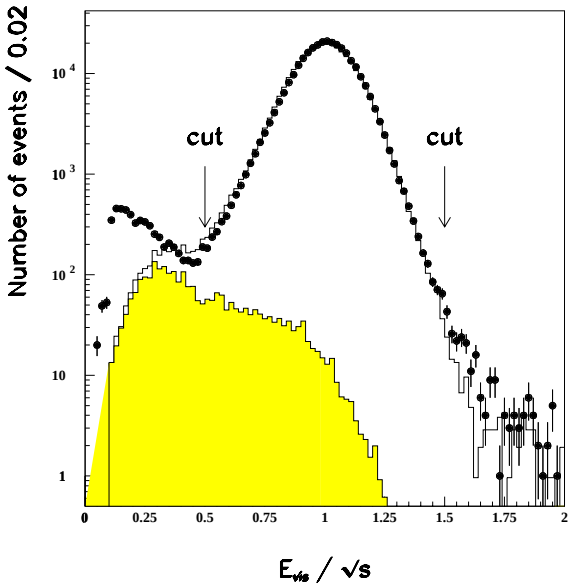

Figure 5.1: Total visible energy divided by the center of mass energy for $e^+e^- \rightarrow$ hadrons compared to Monte Carlo and background distributions from $e^+e^- \rightarrow \tau^+\tau^-(\gamma)$ and $e^+e^- \rightarrow e^+e^-(\gamma)$.

hadronic cross section for each LEP fill. The individual results are statistically compatible and we find no evidence for a time dependence of our measurements.

Adding all uncertainties in quadrature we assign a 0.2% (0.3% in 1990) systematic error to the corrected number of hadronic events.

For an integrated luminosity of 18.2 pb^{-1} we find 422585 $e^+e^- \rightarrow$ hadrons events. The cross sections around the Z resonance are listed in table 5.1. These cross sections have been corrected for acceptance and the finite energy spread of LEP (see section 2.10). The 1991 data are split into two parts reflecting the improved LEP energy calibration after August 14, 1991 [27]. The measurements are compared in figure 5.2a) to the result of the fit to all hadronic and leptonic cross sections as described in section 8.4. The resonance curve of the Z is very well described by our data which can be seen from figure 5.2b) where the ratio of the measured and fitted cross sections is plotted. The points agree within the statistical error.

Data 1990			
$\sqrt{s}$ (GeV)	N_{events}	$\mathcal{L}$ (nb^{-1})	σ_{tot} (nb)
88.231	1776	393.3	4.53±0.11
89.236	3841	453.7	8.50±0.14
90.238	6725	364.0	18.60±0.25
91.230	83835	2784.8	30.38±0.12
92.226	8637	399.5	21.78±0.26
93.228	6368	518.3	12.36±0.16
94.223	3915	480.0	8.20±0.14
Totals	115097	5393.6	

Data 1991			
$\sqrt{s}$ (GeV)	N_{events}	$\mathcal{L}$ (nb^{-1})	σ_{tot} (nb)
91.254	155091	5130.8	30.43±0.10
88.480	4050	782.9	5.17±0.09
89.470	8528	847.9	10.08±0.12
90.228	14333	794.3	18.12±0.18
91.222	90618	3014.8	30.26±0.13
91.967	16059	658.5	24.51±0.24
92.966	10864	759.2	14.36±0.16
93.716	7945	794.6	10.02±0.13
Totals	307488	12783.0	

Table 5.1: Results on the cross section for the reaction $e^+e^- \to$ hadrons. Quoted errors are statistical only; the overall systematic uncertainty in the cross section is 0.2% (0.3% for 1990 data) from the selection and acceptance of the hadronic events and 0.6% from the luminosity measurement.

5.2 The reaction $e^+e^- \to \mu^+\mu^-(\gamma)$

5.2.1 Cross section

The process $e^+e^- \to \mu^+\mu^-(\gamma)$ is identified as an event with two muons in the angular range $|\cos\theta| < 0.8$. In the L3 detector a muon is identified either by its track in the muon chambers or as a minimum ionizing particle in the calorimeters. To suppress cosmic ray background at least one of the muon candidates must have the corresponding scintillation counter fired within 3 ns of the beam crossing or a track in the central tracking chamber with a distance of closest approach to the interaction point of less than 2.5 mm in the $r\phi$ plane.

For events with two reconstructed muons in the muon chambers (81% of the total sample) one muon momentum must exceed $\frac{2}{3}E_{\text{beam}}$. Figure 5.3 shows the momentum distribution of the most energetic muon in the event compared to the Monte Carlo prediction [28] for data

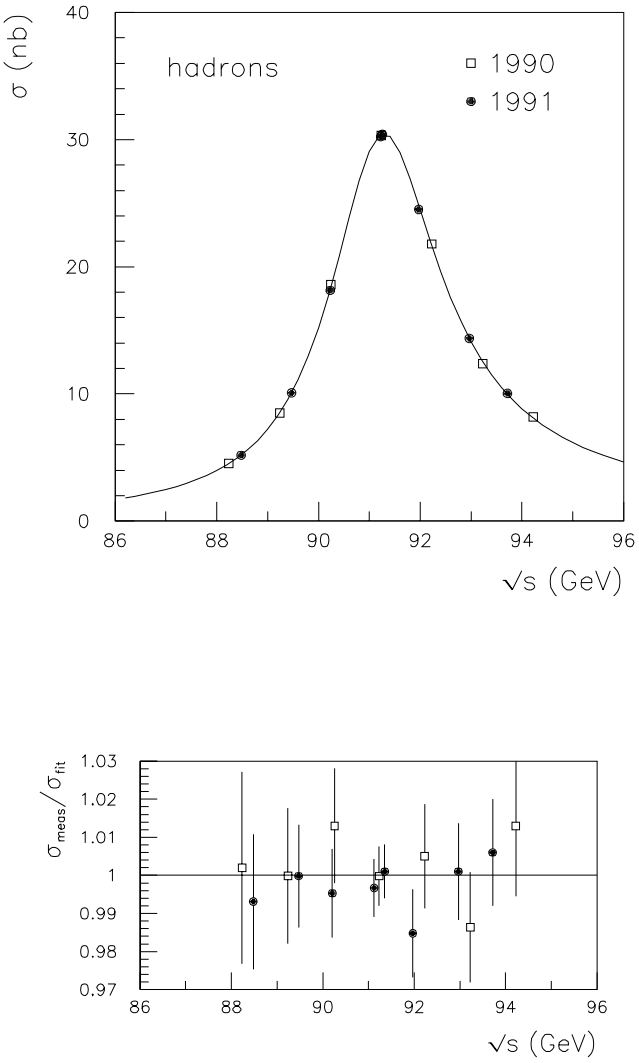

Figure 5.2: a) The total hadronic cross section. b) The ratio of the total hadronic cross section and the fit to all hadronic and leptonic cross sections.

at the Z peak. Good agreement between the data and the Monte Carlo is observed. The momentum cut removes most of the background from $e^+e^- \to \tau^+\tau^-(\gamma)$, two-photon processes and hadronic events. The remaining $e^+e^- \to$ hadrons events are rejected by a charged multiplicity requirement.

The background remaining in the event sample originates from Z decays into $\tau^+\tau^-$ and from cosmic rays. The $e^+e^- \to \tau^+\tau^-(\gamma)$ contamination has been determined to be $(1.7 \pm 0.1)\%$ by analyzing events generated with KORALZ [28]. We have estimated the cosmic ray background by extrapolating the observed rate of events with tracks in the central chamber not pointing to the vertex. We derive a contamination of $(0.7 \pm 0.1)\%$. Other possible background sources are found to be negligible.

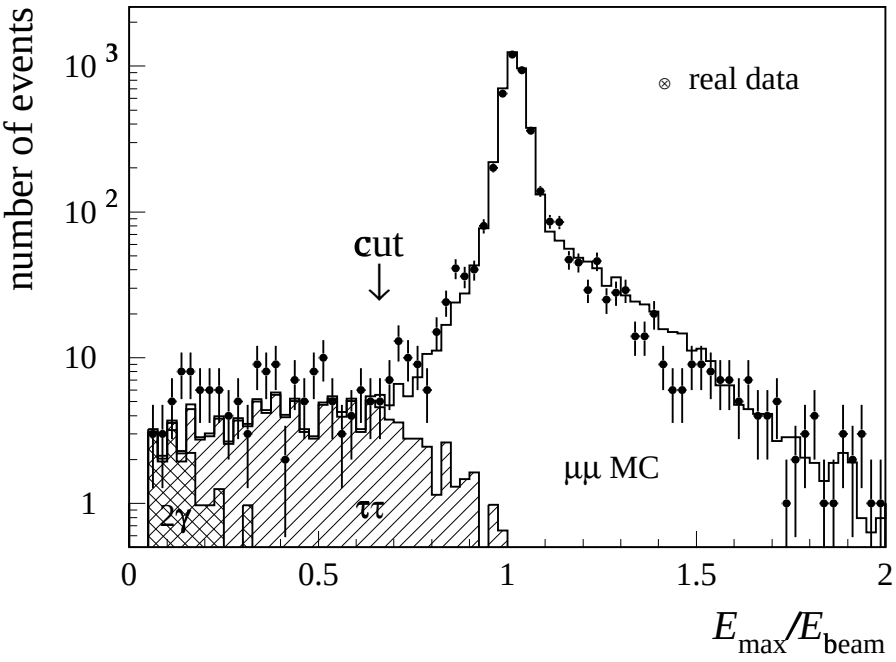

Figure 5.3: The measured momentum of the most energetic muon compared to $e^+e^- \to \mu^+\mu^-(\gamma)$ and background Monte Carlo.

The uncertainty in the event selection has been determined to 0.3% by varying our selection cuts. The acceptance inside the fiducial volume is $(97.58 \pm 0.08)\%$.

The cross section determined in the fiducial volume is extrapolated to the full $\cos\theta$ range. Since the contribution of hard initial state bremsstrahlung is different above and below the Z peak the $\cos\theta$ distribution of the events depends slightly on the center of mass energy. Hence, the fraction of events inside our fiducial volume changes by up to 2% over the energy range of our measurements. We assign a 0.2% error to the extrapolation.

After applying the above selection criteria, 14115 events are selected from the data sample with a total integrated luminosity of 18.1 pb^{-1}. The measured cross sections together with the number of events and the luminosity collected at each energy point are listed in Table 5.2. Figure 5.4 compares the measured cross sections to the result of a fit to all hadronic and leptonic data as described in section 8.4.

5.2.2 Forward-Backward Asymmetry

The forward-backward asymmetry, A_{fb}, is defined as follows:

$$A_{\mathrm{fb}} \equiv \frac{\sigma_F - \sigma_B}{\sigma_F + \sigma_B} \tag{5.1}$$

where σ_F (σ_B) is the cross section for events with the μ^- scattered into the forward (backward) hemisphere with respect to the electron beam direction.

Data 1990			
$\sqrt{s}$ (GeV)	N_{events}	$\mathcal{L}$ (nb^{-1})	σ_{tot} (nb)
88.231	66	388.6	0.268±0.033
89.236	104	421.0	0.387±0.038
90.238	217	364.9	0.929±0.063
91.230	2675	2822.4	1.476±0.028
92.226	282	394.8	1.115±0.066
93.228	160	496.6	0.505±0.040
94.223	123	480.4	0.404±0.036
Totals	3627	5368.7	

Data 1991			
$\sqrt{s}$ (GeV)	N_{events}	$\mathcal{L}$ (nb^{-1})	σ_{tot} (nb)
91.254	5425	5041.9	1.497±0.020
88.480	130	780.4	0.235±0.021
89.470	290	851.1	0.478±0.028
90.228	492	794.3	0.866±0.039
91.222	2912	2933.8	1.381±0.026
91.967	585	700.9	1.165±0.048
92.966	372	759.2	0.686±0.036
93.716	282	830.9	0.478±0.028
Totals	10488	12692.4	

Table 5.2: Results on the cross section for the reaction $e^+e^- \to \mu^+\mu^-(\gamma)$. σ_{tot} is the cross section extrapolated to the full solid angle. Quoted errors are statistical only and the overall systematic uncertainty in the cross section is 0.5% (0.8% for 1990 data), excluding the 0.6% luminosity uncertainty.

For this measurement we use the subsample of events where both muon momenta are measured in the muon chambers. From the fraction of the events where both muons have the same reconstructed charge we determine the charge confusion rate to be $(1.2 \pm 0.2)\%$ for single muons. These events are removed from our sample. The main source for charge confusion are tracks passing close to the edges of the sensitive regions of the muon chambers. Studying the angular distribution of the same charge events we derive a probability of less than 0.2% that both muon charges are wrongly measured which translates into a systematic error of $0.004 A_{\text{fb}}$ due to charge reconstruction.

Events with hard initial state bremsstrahlung are removed from the sample by requiring that the acolinearity angle ζ of the $\mu^+\mu^-$ pair is less than 15°. This allows us to approximate the angular distribution for $|\cos\theta| < 0.8$ with the lowest order form:

$$\frac{d\sigma}{d\cos\theta} \propto \frac{3}{8}(1+\cos^2\theta) + A_{\text{fb}}\cos\theta \tag{5.2}$$

From comparisons to the full electroweak calculations (ZFITTER [29]) we conclude that this approximation translates to a systematic error of less than 0.003 in the determination of the asymmetry. The asymmetry at a given energy point is then determined by a maximum like-

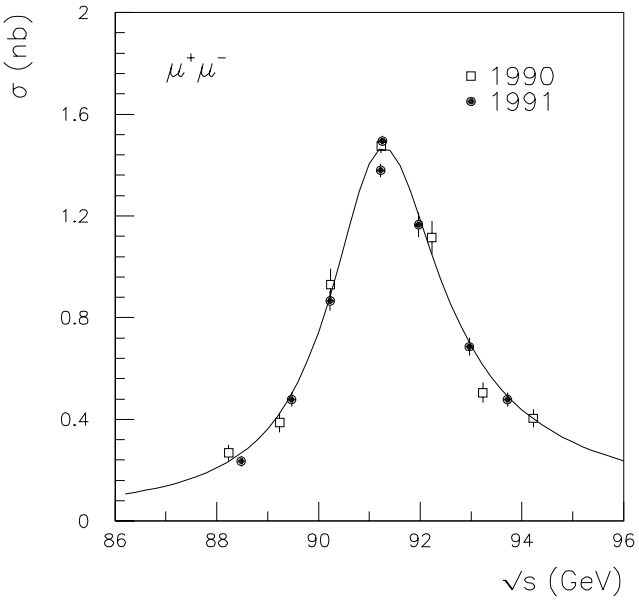

Figure 5.4: The measured muon pair cross section as a function of the center of mass energy.

lihood fit to our data where the likelihood is defined as the product over the selected events weighted with their $\cos\theta_i$ value:

$$L \equiv \prod_i \left(\frac{3}{8}(1+\cos^2\theta_i) + A_{\rm fb}\cos\theta_i \right). \tag{5.3}$$

This method does not require the exact knowledge of the acceptance as a function of the polar angle provided that the acceptance is independent of the muon charge. Comparing the momentum spectra of positively and negatively charged muons we can set a limit of 0.002 on the systematic error on the dimuon asymmetry induced by a possible charge dependence of the muon acceptance.

The background from the reaction $e^+e^- \to \tau^+\tau^-(\gamma)$ in the dimuon sample does not modify the asymmetry since these events have the same forward-backward asymmetry as $e^+e^- \to \mu^+\mu^-(\gamma)$ events. The systematic error from the small cosmic rays background is negligible. In summary, we assign a total systematic error of 0.005 to the asymmetry.

The results for the different center of mass energies are shown in table 5.3 and compared in figure 5.5 to the combined fit result (see section 8.4).

In figure 5.6 we show the angular distribution, corrected for the $\cos\theta$ dependent acceptance, for $\sqrt{s} = 91.22$ GeV. The result for the asymmetry (0.019 ± 0.015) obtained from a fit to this distribution agrees well with our result from the likelihood method.

Data 1990		Data 1991	
$\sqrt{s}$ (GeV)	$A_{\rm fb}$	$\sqrt{s}$ (GeV)	$A_{\rm fb}$
		91.254	0.018±0.015
88.231	-0.39±0.12	88.480	-0.15±0.10
89.236	-0.04±0.11	89.470	-0.20±0.07
90.238	-0.184±0.074	90.228	-0.041±0.052
91.230	0.006±0.021	91.222	0.013±0.021
92.226	0.110±0.066	91.967	0.060±0.045
93.228	0.095±0.091	92.966	0.122±0.058
94.223	0.134±0.099	93.716	0.084±0.067

Table 5.3: Measured forward-backward asymmetry, $A_{\rm fb}$, for the reaction $e^+e^- \to \mu^+\mu^-(\gamma)$ with $\zeta < 15°$. The quoted errors are statistical only. The systematic error is estimated to be less than 0.005.

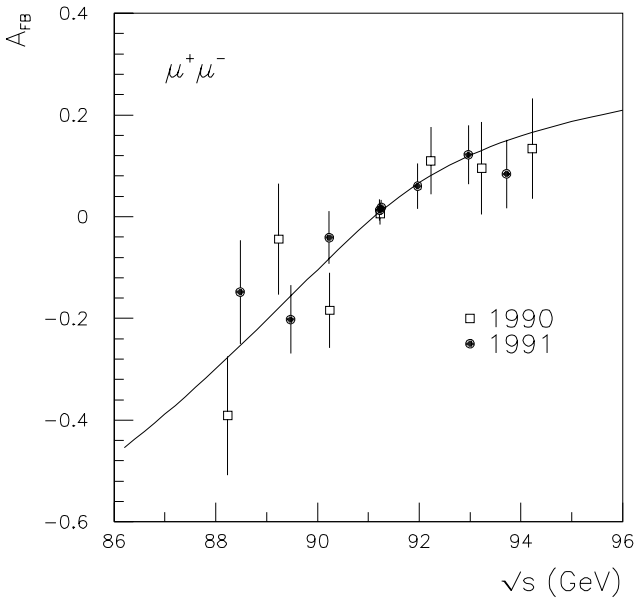

Figure 5.5: The $e^+e^- \to \mu^+\mu^-(\gamma)$ forward-backward asymmetry as a function of the center of mass energy.

5.3 The reaction $e^+e^- \to \tau^+\tau^-(\gamma)$

5.3.1 Cross section

The event selection for $e^+e^- \to \tau^+\tau^-(\gamma)$ is mainly based on calorimetric quantities. Tau pairs are selected in the fiducial volume defined by $|\cos\theta_t| < 0.73$ where the polar angle θ_t is given by the thrust axis of the event. The total energy measured in the electromagnetic and hadron

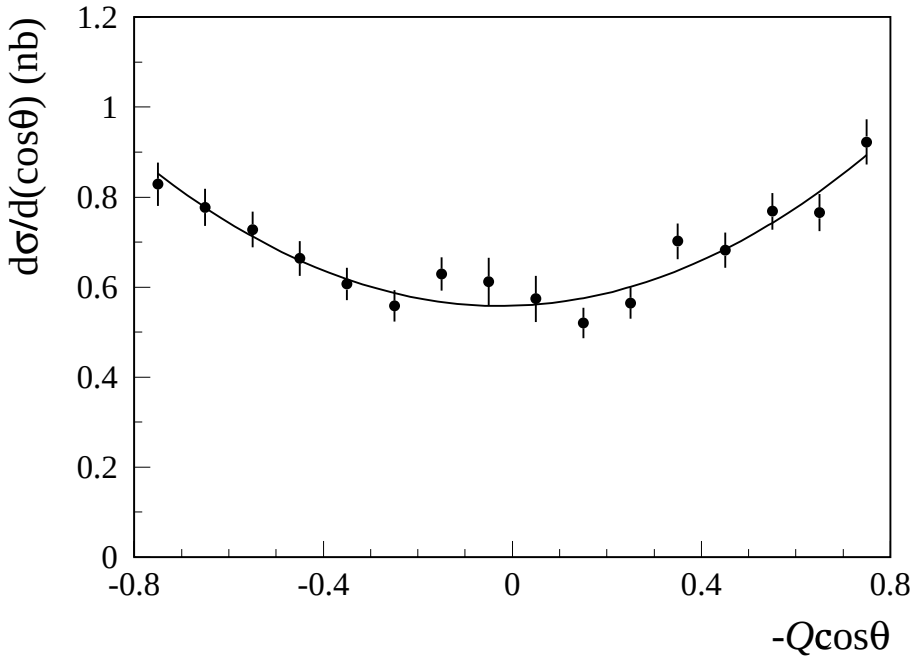

Figure 5.6: The differential cross section of $e^+e^- \rightarrow \mu^+\mu^-(\gamma)$ at the Z peak (91.22 GeV). The solid curve is the result of a fit using equation 5.2.

calorimeters must be above 7 GeV for the most energetic jet and above 3 GeV for the second most energetic jet. The acolinearity angle ζ between the two most energetic jets must be smaller than 250 mrad. To reject cosmic background we require a scintillator fired within 2.5 ns of the beam crossing. The two most energetic clusters in the electromagnetic calorimeter must have energies below 90% and 65% of the beam energy to reject events from $e^+e^- \rightarrow e^+e^-(\gamma)$. Similarly, the momentum measured in the muon chambers must be less than $0.9E_{\rm beam}$ for the most energetic and $0.4E_{\rm beam}$ for the second most energetic muon candidate in the event. Figure 5.7 shows the distributions of the most energetic cluster in the electromagnetic calorimeter and highest momentum muon track for $e^+e^- \rightarrow \tau^+\tau^-(\gamma)$ candidates and background. High multiplicity hadronic Z decays are removed by requiring less than 13 reconstructed energy clusters in the calorimeters. In addition, there should be no track in the central chamber with an azimuthal angle ϕ larger than 250 mrad to the axis of the nearest jet.

In this sample, a background of $(2.70 \pm 0.15)\%$ remains from the other Z decay channels. Smaller contaminations originate from cosmic rays $(0.25 \pm 0.08)\%$ and two-photon processes $(0.12 \pm 0.05)\%$, mainly $e^+e^- \rightarrow e^+e^-e^+e^-$. From varying the selection criteria we derive a systematic error of 0.6%.

The acceptance for $e^+e^- \rightarrow \tau^+\tau^-(\gamma)$ has been determined from Monte Carlo to $(78.05 \pm 0.12)\%$ inside the fiducial volume. Because the acceptance depends on the decay mode, an additional error of 0.2% has to be added due to the uncertainties of the tau branching ratios. In total, we assign a systematic error of 0.7% to the number of $e^+e^- \rightarrow \tau^+\tau^-(\gamma)$ events.

For an integrated luminosity of 17.6 $\rm pb^{-1}$ we find 9943 events. Table 5.4 and figure 5.8 show

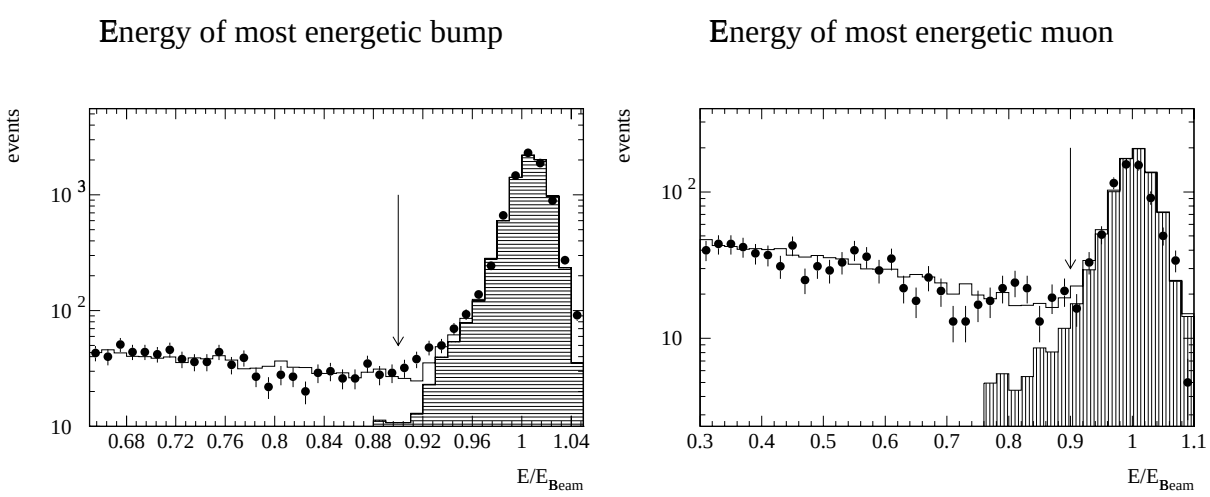

Figure 5.7: The energy of a) the most energetic electromagnetic cluster and b) of the highest momentum muon for $e^+e^- \to \tau^+\tau^-(\gamma)$ candidates compared to $e^+e^- \to \tau^+\tau^-(\gamma)$ and background Monte Carlo.

the results of the $e^+e^- \to \tau^+\tau^-(\gamma)$ cross section measurement. Again, the cross sections have been extrapolated to the full solid angle for each center of mass energy taking into account the variations of the acceptance ($\leq 2\%$).They are compared to the result of a fit to all hadronic and leptonic data as described in section 8.4.

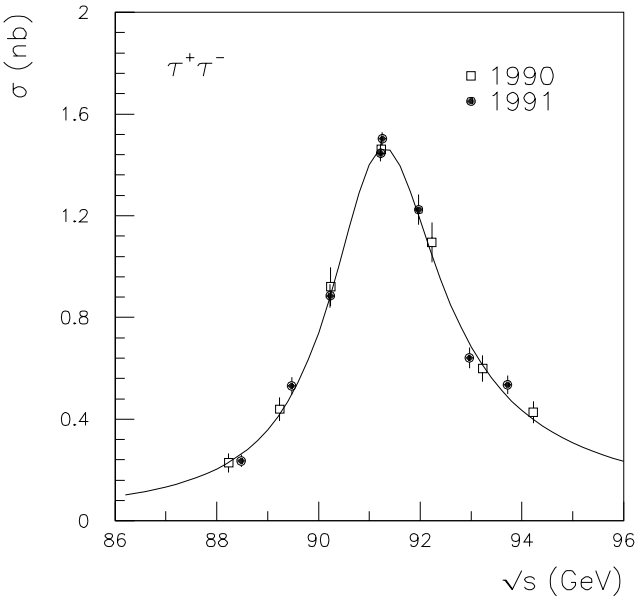

Figure 5.8: The measured tau pair cross section as a function of the center of mass energy.

Data 1990			
$\sqrt{s}$ (GeV)	N_{events}	$\mathcal{L}$ (nb^{-1})	σ_{tot} (nb)
88.231	36	337.8	0.228±0.037
89.236	83	404.7	0.439±0.047
90.238	138	319.9	0.920±0.077
91.230	1868	2721.3	1.463±0.033
92.226	188	366.3	1.095±0.078
93.228	132	472.2	0.599±0.051
94.223	95	477.4	0.427±0.043
Totals	2540	5099.6	

Data 1991			
$\sqrt{s}$ (GeV)	N_{events}	$\mathcal{L}$ (nb^{-1})	σ_{tot} (nb)
91.254	3720	4909.1	1.505±0.025
88.480	95	780.4	0.236±0.024
89.470	229	851.1	0.531±0.035
90.228	359	794.3	0.885±0.047
91.222	2102	2886.1	1.447±0.032
91.967	425	690.2	1.224±0.059
92.966	248	759.2	0.641±0.041
93.716	225	830.9	0.535±0.036
Totals	7403	12501.3	

Table 5.4: Results on the cross sections for the reaction $e^+e^- \to \tau^+\tau^-(\gamma)$. σ_{tot} is the cross section extrapolated to the full solid angle. Quoted errors are statistical only and the overall systematic uncertainty in the cross section is 0.7% (1.5% for 1990 data), excluding the 0.6% luminosity uncertainty.

5.3.2 Forward-Backward Asymmetry

The charge of a tau is determined from the charges of its decay products determined from the curvature of the tracks in the central tracking chamber or in the muon chambers. The sum of all charges in a jet gives the charge of a tau. For the determination of the forward-backward asymmetry we only take events where the two taus have opposite charge. 7441 tau pairs satisfy this additional requirement. We loose mainly events where particles pass through the low resolution regions of the central tracking chamber close to the cathode or anode wire planes. The charge confusion probability is $(10.2 \pm 0.3)\%$ for a single tau. We correct for this and estimate a residual systematic error for the $e^+e^- \to \tau^+\tau^-(\gamma)$ forward-backward asymmetry of $0.001 A_{\text{fb}}$.

The systematic uncertainty due to the subtraction of the $e^+e^- \to e^+e^-(\gamma)$ background is 0.005; due to the cosmic ray background it is 0.001. In total, we assign a systematic error of 0.006 to the measurement of the forward backward asymmetry.

Data 1990		Data 1991	
$\sqrt{s}$ (GeV)	$A_{\rm fb}$	$\sqrt{s}$ (GeV)	$A_{\rm fb}$
		91.254	0.037±0.021
88.231	-0.42±0.20	88.480	-0.11±0.13
89.236	-0.09±0.15	89.470	-0.152±0.083
90.238	-0.18±0.11	90.228	-0.137±0.070
91.230	0.07±0.03	91.222	-0.032±0.029
92.226	-0.04±0.10	91.967	0.042±0.063
93.228	0.11±0.12	92.966	0.161±0.079
94.223	0.02±0.13	93.716	0.058±0.082

Table 5.5: Measured forward-backward asymmetry, $A_{\rm fb}$, of the reaction $e^+e^- \to \tau^+\tau^-(\gamma)$ for $\zeta < 250$ mrad. Quoted errors are statistical only. The systematic error is estimated to be less than 0.006 (0.01 for 1990 data).

The determination of the asymmetry is carried out in the same way as for the $e^+e^- \to \mu^+\mu^-(\gamma)$ events, i.e. independent of the acceptance at each value of $\cos\theta$ (see section 5.2.2). The results are summarized in table 5.5 for the different center of mass energies and compared in figure 5.9 to the result of the combined fit (see section 8.4).

Figure 5.10 shows the acceptance corrected angular distribution of the $e^+e^- \to \tau^+\tau^-(\gamma)$ events collected on the Z peak.

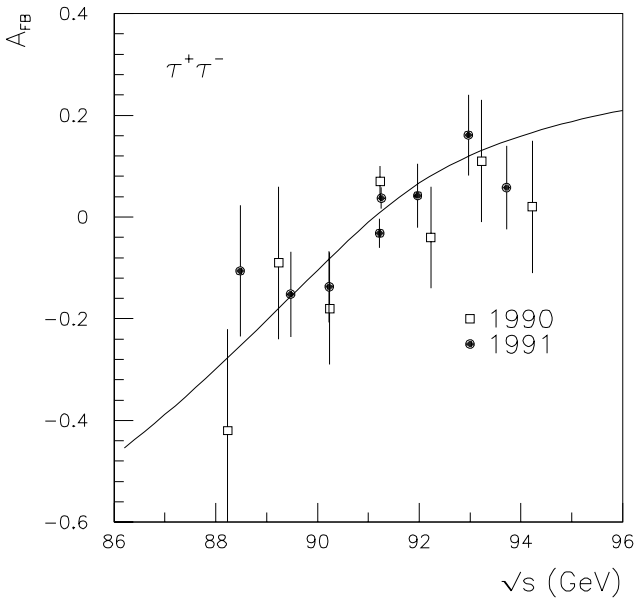

Figure 5.9: The $e^+e^- \to \tau^+\tau^-(\gamma)$ forward-backward asymmetry as a function of the center of mass energy.

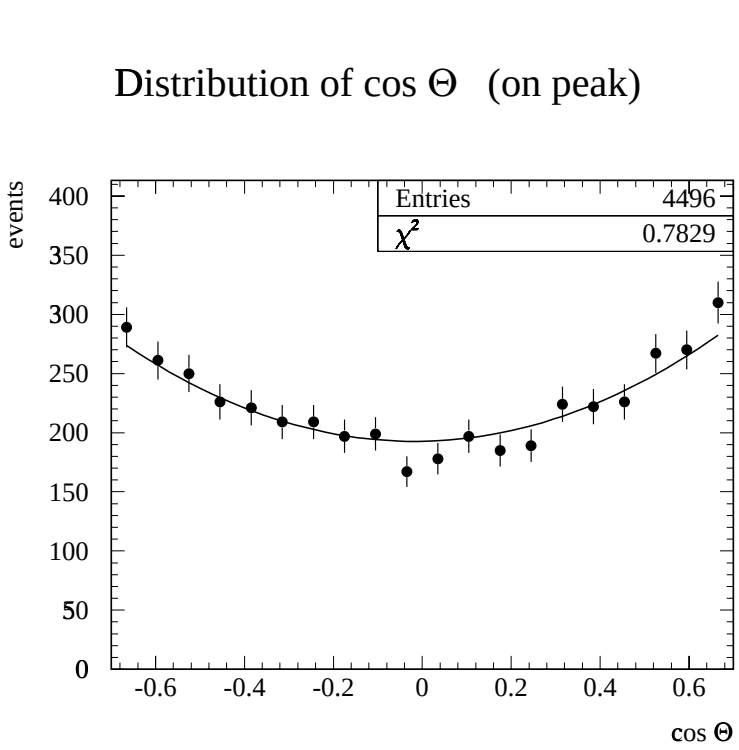

Figure 5.10: The angular distribution of $e^+e^- \to \tau^+\tau^-(\gamma)$ at the Z peak. The data are compared to the results of a fit using equation 5.2.

5.4 The reaction $e^+e^- \to e^+e^-(\gamma)$

5.4.1 Cross section

We select $e^+e^- \to e^+e^-(\gamma)$ events based on the energy deposition in the barrel part of the electromagnetic calorimeter. The fiducial volume for this analysis is thus defined by $44° < \theta < 136°$ which excludes crystals at the edges of the barrel calorimeter. Hadronic Z decays are suppressed requiring that the events have less than 8 reconstructed clusters in the electromagnetic calorimeter. To reject tau pair events, we require that $E_1 > 0.85 E_{\rm beam}$ and $E_2 > 2$ GeV, where E_1 and E_2 are the energies of the two most energetic clusters in the electromagnetic calorimeter. Figure 5.11 illustrates the cut on the most energetic cluster and the good agreement of our data and the Monte Carlo simulation. The acolinearity angle ζ between the two most energetic clusters must be less than 25° to reduce the effect of hard initial state bremsstrahlung. The only sizable background remaining after these cut is a $(1.5 \pm 0.1)\%$ contamination of $e^+e^- \to \tau^+\tau^-(\gamma)$ events and a 16.4 pb background of $e^+e^- \to \gamma\gamma(\gamma)$ events at the Z peak.

Inside the fiducial volume and for $\zeta < 25°$, the acceptance is determined for $e^+e^- \to e^+e^-(\gamma)$ using events generated with BABAMC [30, 31]. Including detector inefficiencies we find an acceptance of $(99.5 \pm 0.1)\%$. We use events generated with the program BHAGENE [32] to estimate the effects of double radiative events $e^+e^- \to e^+e^-\gamma\gamma$ on our selection efficiency. The cut on E_1 introduces an additional inefficiency of 0.3% due to the presence of a second hard photon. From variations of the energy, fiducial volume and acolinearity cut we derive a

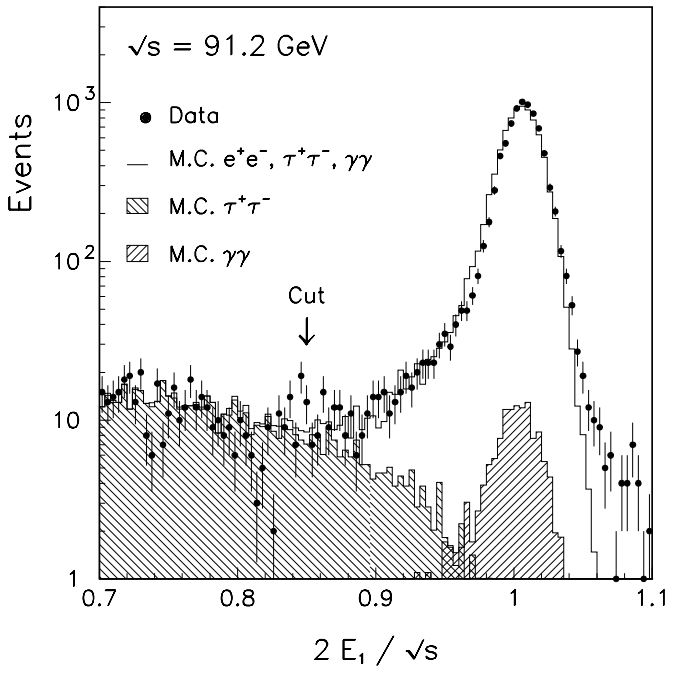

Figure 5.11: The most energetic cluster in the electromagnetic calorimeter compared to $e^+e^- \to e^+e^-(\gamma)$ and background Monte Carlos.

systematic error of 0.3% for the selection of events. Adding the uncertainties from background subtraction (0.1%) and Monte Carlo statistics (0.1%) we assign a systematic error of 0.4% to the corrected number of $e^+e^- \to e^+e^-(\gamma)$ events inside the fiducial volume. The measured cross sections are listed in table 5.6.

The exchange of time-like and space-like photons and Z bosons contribute to the cross section of $e^+e^- \to e^+e^-(\gamma)$. To extract the Z resonance contribution two methods can be used. The measured cross sections in a given fiducial volume can be directly compared to a theoretical calculation which includes all contributing Feynman diagrams, e.g. 40THIEVES [33], ALIBABA [34] or BHAGENE [32]. Alternatively, the ratio $\sigma_s/\sigma_{\rm tot}$ can be evaluated using the above programs to scale the measured cross sections. After this correction the Z decay into e^+e^- can be treated like the other decay channels. Both methods lead to consistent results.

We use the ALIBABA program to calculate the contributions from the t channel and the interference of the t and s channel. Figure 5.12 shows the total cross section for $44^\circ < \theta < 136^\circ$ and for an acolinearity angle of less than 25°. The measurements are compared to the calculation with ALIBABA using the Standard Model parameters determined in section 8.4. The calculated contributions from s channel and non-s channel are shown separately. Comparing different theoretical calculations we conclude that the non-s channel subtraction and the extrapolation to the full solid angle leads to a systematic error of 0.5%, including the 0.4% experimental error discussed above. The extrapolated cross sections can be found in table 5.6.

Data 1990				
$\sqrt{s}$ (GeV)	N_{events}	$\mathcal{L}$ (nb^{-1})	σ_{tot} (nb)	σ_s (nb)
88.231	120	380.1	0.334±0.030	0.188±0.053
89.236	237	466.3	0.532±0.034	0.473±0.057
90.238	310	359.3	0.894±0.050	1.034±0.082
91.230	3020	2960.9	1.052±0.019	1.462±0.031
92.226	276	397.4	0.715±0.043	1.135±0.071
93.228	198	505.5	0.405±0.029	0.660±0.048
94.223	104	485.7	0.223±0.022	0.348±0.037
Totals	4265	5555.2		

Data 1991				
$\sqrt{s}$ (GeV)	N_{events}	$\mathcal{L}$ (nb^{-1})	σ_{tot} (nb)	σ_s (nb)
91.254	5422	5244.3	1.031±0.014	1.437±0.023
88.480	316	783.5	0.400±0.023	0.291±0.040
89.470	498	862.3	0.573±0.026	0.528±0.044
90.228	632	795.0	0.792±0.032	0.866±0.053
91.222	3295	3080.8	1.067±0.019	1.484±0.030
91.967	591	731.7	0.798±0.033	1.239±0.054
92.966	336	759.9	0.430±0.024	0.701±0.040
93.716	261	832.1	0.302±0.019	0.486±0.032
Totals	11351	13089.6		

Table 5.6: Results on the cross section for the reaction $e^+e^- \to e^+e^-(\gamma)$. σ_{tot} is the acceptance corrected cross section for $44° < \theta < 136°$ and $\zeta < 25°$. σ_s is the s-channel corrected cross section extrapolated to the full solid angle as explained in the text. The quoted errors are statistical only and the overall systematic uncertainty, excluding the 0.6% luminosity uncertainty, in the cross section is 0.4% for σ_{tot} and 0.5% for σ_s.

5.4.2 Forward-Backward Asymmetry

For the measurement of the forward-backward asymmetry we use the polar angle θ of the scattered e^-, as determined from the reconstructed center of the energy cluster in the electromagnetic calorimeter. The angular resolution of 1.2° is dominated by the longitudinal extension of the LEP bunches of about ±1 cm.

The charges of the outgoing particles are determined in the central tracking chamber. We require the two electromagnetic clusters to be matched to tracks within 25 mrad, in the plane transverse to the beam direction. Since the length of an electron or positron track in the central tracking chamber is only $31\text{cm}/\cos\theta$ a measurement of the curvature of each track leads to a momentum resolution of 100% at 45 GeV. This measurement is substantially improved by including the reconstructed impact points of the particles onto the electromagnetic calorimeter.

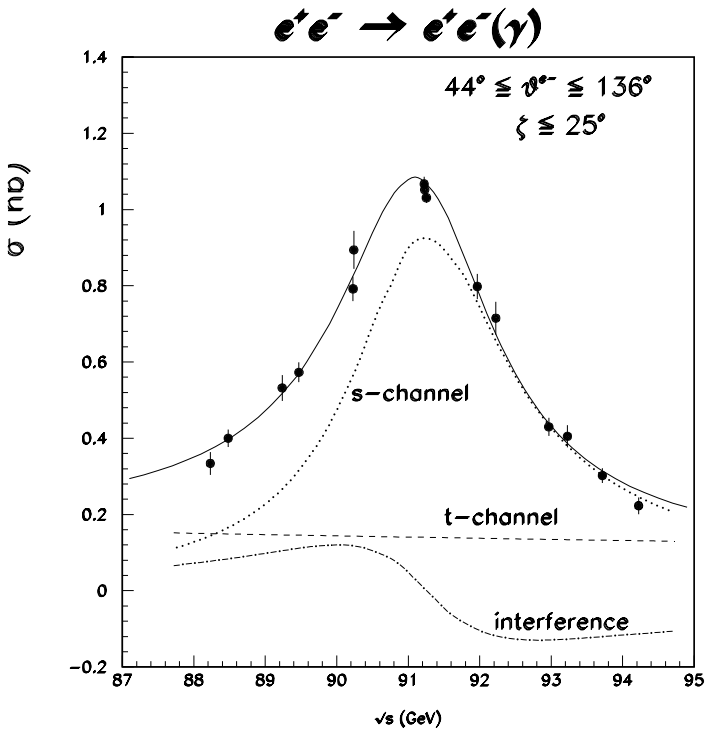

Figure 5.12: The $e^+e^- \to e^+e^-(\gamma)$ cross section for $44° < \theta < 136°$ and $\zeta < 25°$ compared to the ALIBABA calculation. The contributions from s and t channel are shown separately.

We check this method by applying the same procedure to the selected $e^+e^- \to \mu^+\mu^-(\gamma)$ sample and comparing the charge assignment of the events by the central tracking chamber and by the muon spectrometer. We find that in $(4.3 \pm 0.3)\%$ of the events the charge is assigned wrongly.

The asymmetry is defined by counting the events in the forward ($44° < \theta < 90°$) and backward ($90° < \theta < 136°$) hemispheres. The data are corrected bin-by-bin for the $\cos\theta$ dependent acceptance and charge confusion. The systematic error on the asymmetry is estimated to 0.004. In Table 5.7 the measured asymmetry is given at each energy point. In Figure 5.13 the differential cross section at the Z peak is shown as a function of $\cos\theta$.

The pure s channel forward-backward asymmetry A^s_{FB} can be extracted in a similar way to the muon and tau asymmetries using a likelihood fit. The non-s channel contribution to the angular distributions are parameterized by a function $\Omega(\cos\theta)$ calculated with the help of the ALIBABA program for each $\sqrt{s}$ point. We build the following likelihood function :

$$L \equiv \prod_i \left(\frac{3}{8}(1 + \cos^2\theta_i) + A^s_{FB} \cos\theta_i + \Omega(\cos\theta_i) \right). \tag{5.4}$$

The effects of the charge confusion are taken into account in the likelihood function. The precision of the ALIBABA program and the dependence of $\Omega(\cos\theta_i)$ on the Z and top quark masses lead to an additional systematic error of 0.003 on A^s_{FB}. The extrapolated s channel asymmetries are listed in table 5.7 and shown in Figure 5.14 as a function of $\sqrt{s}$. The numbers are corrected for the acolinearity cut.

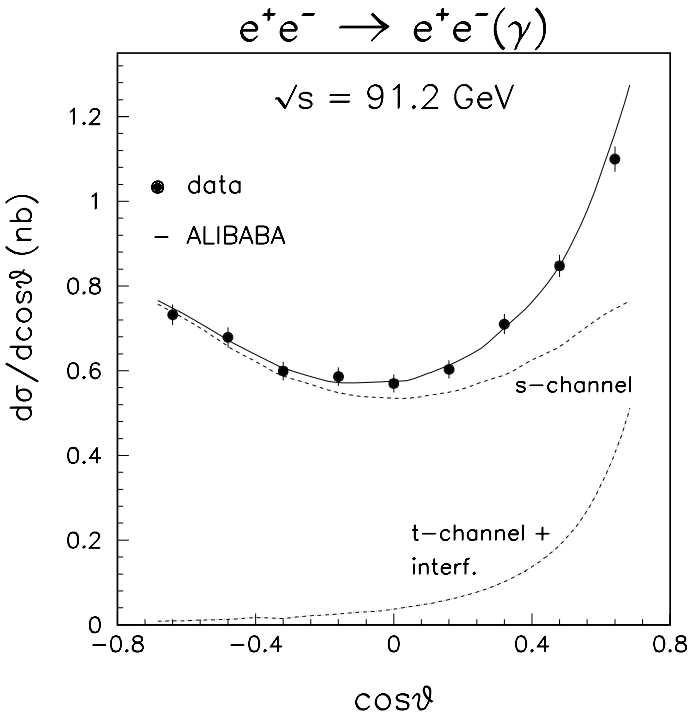

Figure 5.13: The differential cross section of $e^+e^- \rightarrow e^+e^-(\gamma)$ at the Z peak. The data are compared to the ALIBABA program. The contributions from s and t channel are shown separately.

5.5 The reaction $e^+e^- \rightarrow$ hadrons $+ \gamma$

Isolated hard photons produced in hadronic Z decays are mainly associated with radiation from the primary quark-antiquark pair. These events provide information about the electroweak couplings of quarks [35, 36], and serve as probes of the short-distance structure of QCD. LEP is an ideal laboratory for this study because the background from photons radiated from the initial state electrons or positrons is strongly suppressed at the Z resonance. Nonetheless, one must still contend with a significant background from high-energy neutral hadrons, mainly π^0 mesons decaying into two unresolved photons.

We select hadronic events according to the criteria in section 5.1, with the additional requirement that the center-of-mass energy be in the range $91.0 - 91.5$ GeV, in order to reduce the contribution from initial-state photons and interference between initial and final state radiation.

We identify photon candidates in hadronic events as clusters in the barrel region of the electromagnetic calorimeter where the contribution from initial-state photons is minimal, with energy greater than 5 GeV. We also require that photon candidates are not associated with a charged track, and are isolated by at least 15° from other electromagnetic-calorimeter clusters of energy greater than 500 MeV. Finally, jets are reconstructed from the hadronic part of the event (excluding the photon candidate) using the JADE algorithm [37] with the parameter $y_{\rm cut} = 0.05$ (see section 10.2.1). We require that photon candidates be isolated by more than 20° from the axis of each reconstructed jet.

Data 1990		
$\sqrt{s}$ (GeV)	$A_{\rm fb}$	$A^s_{\rm fb}$
88.231	0.520±0.095	-0.034±0.276
89.236	0.296±0.070	-0.205±0.161
90.238	0.155±0.064	-0.111±0.107
91.230	0.101±0.021	-0.023±0.028
92.226	0.040±0.069	0.042±0.085
93.228	0.083±0.081	0.053±0.094
94.223	0.144±0.118	0.129±0.148

Data 1991		
$\sqrt{s}$ (GeV)	$A_{\rm fb}$	$A^s_{\rm fb}$
91.254	0.118±0.014	0.001±0.020
88.480	0.504±0.055	-0.013±0.157
89.470	0.312±0.048	-0.126±0.099
90.228	0.206±0.045	-0.100±0.075
91.222	0.129±0.019	0.019±0.027
91.967	0.161±0.047	0.103±0.055
92.966	0.107±0.064	0.098±0.072
93.716	0.185±0.070	0.165±0.085

Table 5.7: Results on the forward-backward asymmetry for the reaction $e^+e^- \to e^+e^-(\gamma)$. $A_{\rm fb}$ is the asymmetry determined from counting in angular range $44^\circ < \theta < 136^\circ$ and for $\zeta < 25^\circ$. A^s_{FB} is the s channel contribution to the forward-backward asymmetry extrapolated to the full solid angle. The systematic error for each energy point is 0.004 on A_{FB} and 0.005 on A^s_{FB}, respectively.

We find 3202 events with isolated hard photon candidates. Monte Carlo studies indicate that in addition to final-state photons radiated from quarks, our sample includes neutral hadrons (mainly π^0) occurring either as single isolated particles or in tight groups of particles that decay into adjacent photons, as well as a smaller fraction of initial-state photons. We estimate the initial-state radiation contribution to be $69 \pm 5(stat) \pm 15(syst)$ events. To study the remaining background from neutral hadrons, we construct a cluster-shape parameter, C, sensitive to the detailed energy sharing between the BGO crystals in an electromagnetic energy cluster [38]. A fit of the C-distributions for JETSET 7.3 signal and background to the data determines a signal of 848 ± 55 events, corresponding to a direct photon ratio between data and JETSET 7.3 of $R_s = 1.14 \pm 0.06$ $(stat)$. For the background, we find $R_b = 1.88 \pm 0.08$ (stat).

The data distributions are corrected for detector effects, acceptance, and initial state radiation. We then correct for the remaining neutral hadron background by subtracting the JETSET prediction scaled by the factor $R_b = 1.88$ mentioned above. We obtain the fraction of hadronic events with photons isolated by more than 20° from jets and with energy greater than 5 GeV to be

$$\mathrm{Br(Z \to hadrons + \gamma)/Br(Z \to hadrons)} = (5.2 \pm 0.3 \pm 0.4) \times 10^{-3} \ , \qquad (5.5)$$

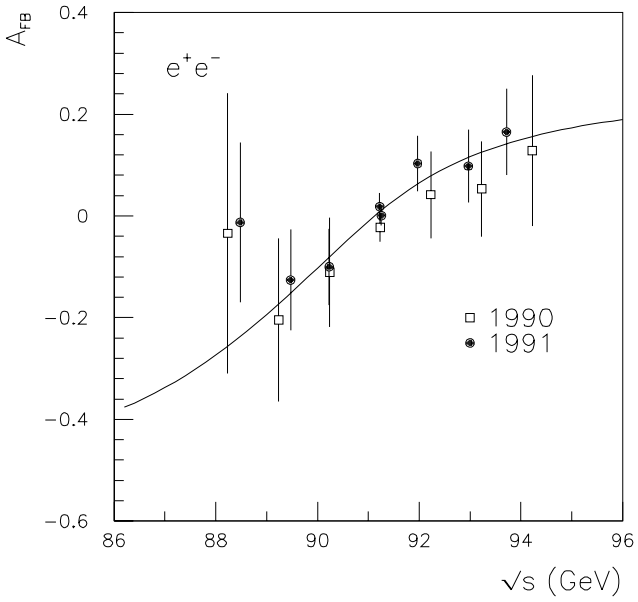

Figure 5.14: The s channel contribution to the $e^+e^- \to e^+e^-(\gamma)$ forward-backward asymmetry as a function of the center of mass energy.

where the first error is statistical and the second error is systematic. The main contribution to the systematic error stems from the uncertainty in the background subtraction [38]. Our result agrees with those of other LEP collaborations [39]. The measured rate will be used in section 8.7.2 to extract separate electroweak couplings to up-type and down-type quarks.

5.6 The reaction $e^+e^- \to \nu\bar{\nu}\gamma$

A direct method for measuring the Z width into neutrinos and thus for counting the number of light neutrino types, is based on the measurement of the cross section for the radiative process $e^+e^- \to \nu\bar{\nu}\gamma$. The signature of such events is a single photon arising from initial state radiation. Around the Z pole the photons from $\nu\bar{\nu}\gamma$ have low energies with a rapidly falling spectrum.

The measurement is optimally carried out at energies at least 3 GeV above the Z mass where the ratio between the signal and QED background processes is maximum and the full width of the Z resonance is exploited [40, 41]. However, the LEP scanning strategy at the Z resonance [42] has given less favorable conditions for our first measurements, requiring a trigger efficient for low energy photons ($E > 1$ GeV), a good knowledge of the electromagnetic energy scale and tight control of backgrounds.

5.6.1 Experimental Procedure

The signature for the reaction $e^+e^- \to \nu\bar{\nu}\gamma$ is a single electromagnetic shower and nothing else observed in the detector. Candidates are selected by requiring:

- a single shower in the electromagnetic calorimeter barrel, with $E > 0.9$ GeV and the characteristics of an electromagnetic shower;
- no muon candidate, no track in the central detector and only small energy deposits in the other calorimeters, including the luminosity monitor;
- no cosmic muon emitting a hard bremsstrahlung and faking a single photon event.

These criteria leave us with 291 candidates from the 1991 running periods, corresponding to an integrated luminosity of 9.6 pb^{-1} [23].

Events of this kind are triggerd by the single photon trigger (see section 2.9). The efficiency for this trigger as a function of the photon energy has been calculated by Monte Carlo. The result is shown in Fig. 5.15. The calculation is verified in absolute value as well as energy dependence by observing events from the process $e^+e^- \to e^+e^-(\gamma)$ with a single large angle electron – selected with criteria analogous to those for the process above – in coincidence with a high energy electromagnetic shower in one of the luminosity monitor calorimeters. The trigger efficiency derived from this sample is also shown in Fig. 5.15 and agrees well with the calculation.

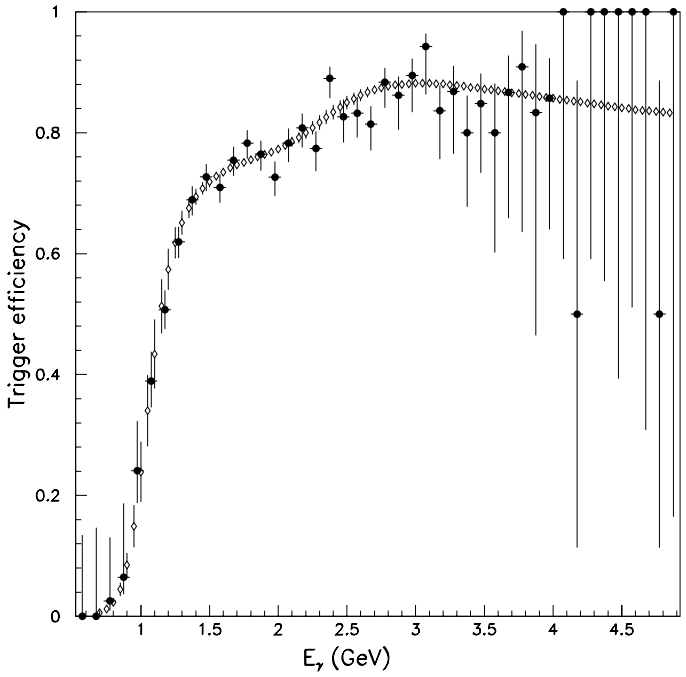

Figure 5.15: The trigger efficiency for $e^+e^- \to \nu\bar{\nu}\gamma$.

The measurement of this process also verifies the Monte Carlo program [43] used to calculate the dominant background, which comes from the process of radiative Bhabha scattering when only the photon is observed in the detector. It is found that a background of 94 ± 10 events is contained in the abovementioned sample.

Residual background from cosmic rays is estimated from a sample of events where cosmic ray rejection was released. Extrapolation to the tighter criteria used for the final selection leads to an estimated background of 1.0 ± 0.8 events. Other backgrounds from radiative processes are estimated by Monte Carlo calculation. These are photons coming from the decay of resonances produced via two-photon processes and the reactions $e^+e^- \to \gamma\gamma\gamma$ and $e^+e^- \to \mu^+\mu^-\gamma$ (15 ± 4 events). Other backgrounds are found to be negligible.

The measured single photon energy distribution for all center of mass energies is shown in Fig. 5.16 along with Monte Carlo predictions for the process $e^+e^- \to \nu\bar{\nu}\gamma$, assuming three families of light neutrinos, for the $e^+e^- \to e^+e^-\gamma$ background and the sum of all other backgrounds. There is good agreement between data and the prediction.

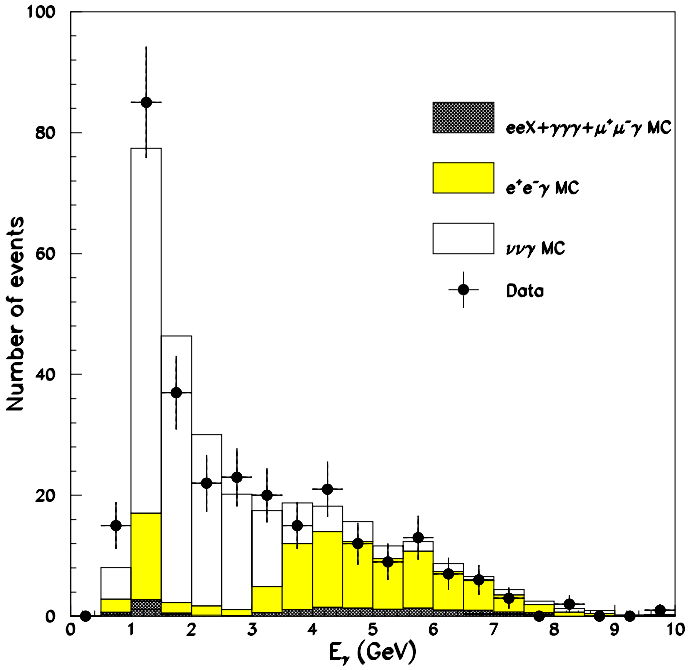

Figure 5.16: Photon energy distribution of $e^+e^- \to \nu\bar{\nu}\gamma$ events.

5.6.2 Cross Section Results

The total cross section is extracted from the number of candidates in the energy range $0.9 < E_\gamma < 3.5$ GeV, where the signal over background ratio is favorable.

For this energy range, table 5.8 shows the luminosity, the number of candidates and the $\nu\bar{\nu}\gamma$ expectations for 3 neutrino families computed with the Monte Carlo NNGSTR [44]. Also

$E_{\rm cm}$ (GeV)	$\mathcal{L}$ (nb^{-1})	$N_{\rm observed}$	$N^{\nu\bar{\nu}\gamma}_{\rm expected}$	$N^{\rm e^+e^-}_{\rm expected}$	$N^{\rm other\ back.}_{\rm expected}$	σ (pb)
88.56	671	6	2.21	1.96	0.35	12^{+12}_{-5}
89.55	772	9	4.27	2.22	0.39	18^{+11}_{-6}
90.25	632	11	5.16	1.78	0.32	31^{+15}_{-8}
91.25	5763	116	92.41	14.42	2.96	37 ± 4
92.04	635	21	17.59	1.72	0.31	64^{+19}_{-12}
93.05	678	26	29.63	1.80	0.33	66^{+17}_{-12}
93.75	419	13	18.35	1.10	0.21	52^{+21}_{-12}
Total	9570	202	169.6	25.0	4.9	

Table 5.8: Luminosity, observed and expected number of events and corrected cross section for $e^+e^- \to \nu\bar{\nu}\gamma$ at each center of mass energy.

shown is the expected background from radiative Bhabha events and, as other backgrounds, the total number of expected events from two-photon processes, from $e^+e^- \to \gamma\gamma\gamma$ and from $e^+e^- \to \mu^+\mu^-\gamma$.

The last column of table 5.8 shows the measured cross sections corrected for acceptances and detector efficiencies for the process $e^+e^- \to \nu\bar{\nu}\gamma$ when one photon is emitted with energy above 0.9 GeV and a polar angle between 45° and 135° without restrictions on possibly additional photons. The errors are only statistical and take into account the uncertainty in the background subtraction.

We extract the number of light neutrino families N_ν by performing a maximum likelihood fit to the number of candidates shown in table 5.8. We use Poisson probabilities calculated as a function of the expected number of signal plus background events. We compute for each center of mass energy the cross section corresponding to different values of N_ν between 2 and 4 and use a straight line fit to get a parameterization of the cross section dependence on N_ν. We use an improved Born approximation of the analytical calculation of reference 45, which agrees with NNGSTR for $N_\nu = 3$ to better than 1% when a coherent set of input parameters is used. In this approach, we can allow the parameter N_ν to vary while keeping the total width fixed. The cross section $\sigma_0(s)$ can be written as

$$\sigma_0(s) = \frac{12\pi}{m_{\rm Z}^2} \frac{s\Gamma_{\rm e} N_\nu \Gamma_{\nu\bar{\nu}}}{(s-m_{\rm Z}^2)^2 + s^2\Gamma_{\rm Z}^2/m_{\rm Z}^2} \quad + \text{W terms} \tag{5.6}$$

where $\Gamma_{\nu\bar{\nu}}$ is the decay width of the Z in a neutrino pair with standard model couplings and $m_{\rm Z}$, $\Gamma_{\rm Z}$, and $\Gamma_{\rm e}$ are our measured values [24], respectively for the Z mass, the total width and the electron partial width. The terms due to W exchange in the t channel and interference between these and the s channel Z exchange contribute less than 3% to the total cross section in the energy range covered here. The results of the fit gives $N_\nu = 3.14 \pm 0.24$ (stat.).

The systematic errors in our analysis come from the determination of the trigger efficiency, which gives an uncertainty of $\Delta N_\nu = \pm 0.04$, from the luminosity measurement, $\Delta N_\nu = \pm 0.03$, the determination of the selection efficiency, $\Delta N_\nu = \pm 0.02$, the background subtraction, $\Delta N_\nu = \pm 0.09$, and the cosmic ray contamination, $\Delta N_\nu = \pm 0.02$. From the errors on our measurements of the Z parameters $m_{\rm Z}$, $\Gamma_{\rm Z}$, and $\Gamma_{\rm e}$, from the top mass variation and the theoretical uncertainty on the parameterization of the cross section, we estimate a contribution to the systematic error

of $\Delta N_\nu = \pm 0.05$. Adding all these systematic errors in quadrature, our final result is

$$N_\nu = 3.14 \pm 0.24(\text{stat.}) \pm 0.12(\text{syst.}). \tag{5.7}$$

This corresponds to an invisible width of the Z of

$$\Gamma_Z^{\text{inv}} = 524 \pm 40(\text{stat.}) \pm 20(\text{syst.}). \tag{5.8}$$

This is in agreement with our previously published result [46] and with the one published by the OPAL collaboration in a similar analysis [47]. The corrected cross section is shown in figure 5.17 as a function of the c.m. energy along with the expectations from $N_\nu = 2, 3, 4$ and from our best fit.

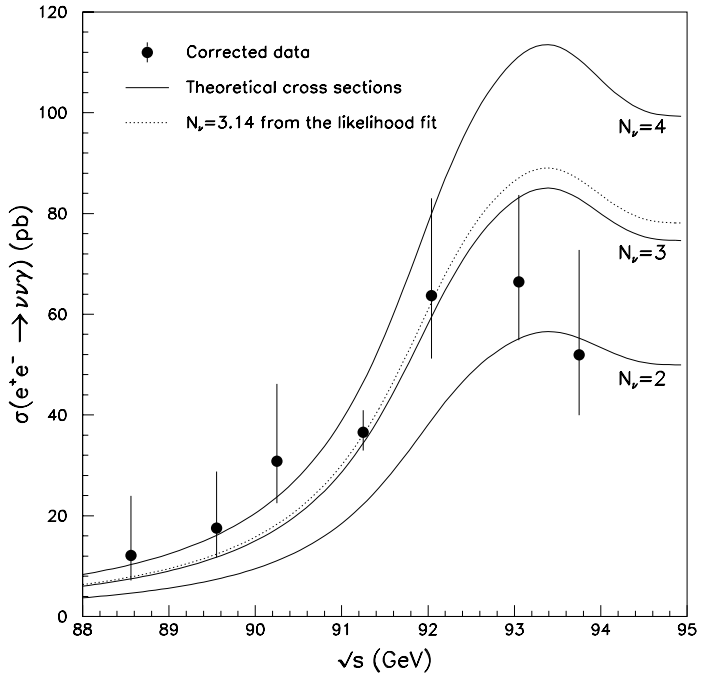

Figure 5.17: Cross section for $e^+e^- \to \nu\bar{\nu}\gamma$ as a function of the center of mass energy.